Exploring *Strobilanthes crispus* as a Sustainable Corrosion Inhibitor for Aluminium: Electrochemical Insight Across pH Variations

Yasin Albarqouni[1,2], Wan Salwanis Binti Wan Md Zain[1], Augustine Agi[1], and Arman Bin Abdullah[1*]

[1]*Faculty of Chemical and Process Engineering Technology, Universiti Malaysia Pahang Al-Sultan Abdullah, Lebuhraya Persiaran Tun Khalil Yaakob, 26300 Kuantan, Pahang, Malaysia*

[2]*Department of Clinical Nutrition, Faculty of Applied Medical Sciences, Al-Azhar University-Gaza (AUG), Gaza City, Gaza Strip 00970, State of Palestine*

* ***Corresponding author:***

email: armanabdullah@umpsa.edu.my

Received: April 8, 2025
Accepted: August 29, 2025

DOI: 10.22146/ijc.105858

Abstract: Strobilanthes crispus *leaf extract was investigated as a green corrosion inhibitor for aluminium in varying pH media (HCl pH 2, NaCl pH 7, NaOH pH 10). FTIR confirmed C–O and C=O functional groups are critical for inhibition. Weight loss measurements after 20 d in NaOH showed corrosion rates of 0.00061 mm/y at 0.2 mg/L inhibitor and 0.00038 mm/y at 0.8 mg/L, with efficiencies of 46.8 and 67.05%, respectively. Inhibition was weaker in NaCl (0.0003–0.0024 mm/y) and HCl (0.0037–0.0005 mm/y). Tafel polarization revealed a reduced corrosion rate in NaOH (0.00022 mm/y vs. 0.019 mm/y uninhibited) and a positive* E_{corr} *shift. EIS demonstrated peak efficiency (75.5% at 0.8 mg/L in NaOH), supported by high charge transfer resistance* R_{ct} *with about* $6.80 \times 10^4\ \Omega$ *and oxide film resistance* R_{of} *with about* $1.19 \times 10^6\ \Omega$*. SEM confirmed smoother surfaces in inhibited NaOH versus pitting in blanks. The extract's efficacy in alkaline conditions rivals that of plant-derived inhibitors, though neutral/acidic performance was limited. These findings position* S. crispus *as a sustainable inhibitor for alkaline environments.*

Keywords: Strobilanthes crispus *extract; corrosion inhibition; green inhibitor*

■ INTRODUCTION

One of the most abundant metals on earth is aluminium. It is used extensively in a variety of applications, including aerospace and marine. However, aluminum corrosion is a costly and enduring problem due to its superior mechanical qualities and lightweight nature [1-2]. Nevertheless, developing efficient and long-lasting corrosion inhibition technologies is necessary because aluminium is susceptible to corrosion in acidic and alkaline media. Traditional corrosion inhibitors, often based on toxic synthetic chemicals such as chromates, cadmium, lead, and organic compounds like hydrazine or formaldehyde [3-5], pose environmental and health risks, leading researchers to explore greener alternatives such as plant-based inhibitors [6].

Plant-based extracts have drawn a lot of interest as possible corrosion inhibitors due to their abundance, affordability, and environmental friendliness [7]. Among these extracts are various phytochemicals, including phenolic compounds, flavonoids, alkaloids, and tannins, which adsorb onto metal surfaces to form protective layers, thereby inhibiting corrosion [8-9]. Previous studies have demonstrated that plant-based inhibitors can significantly reduce corrosion rates by forming stable complexes with metal ions, thereby preventing further oxidation and degradation. For instance, polyphenols, including catechins and gallic acid [10]; flavonoids, including quercetin and rutin [11]; alkaloids including caffeine and piperine [12], exhibit corrosion inhibition through multiple mechanisms. The polar functional groups (OH, CO_2H, NH_2) in these compounds facilitate adsorption onto metal surfaces, forming a protective film that blocks corrosive agents (O_2, Cl^-, H^+) while donating electrons to vacant d-orbitals of metals [13-14]. Green tea, among them, shows a high retention in corrosion rate in acidic media [15].

Strobilanthes crispus, a widely available medicinal plant in Malaysia and Indonesia, exhibits antioxidant and metal-chelating properties, which may help combat diseases such as hepatocellular carcinoma [16], a primary liver cancer originating in the liver [17], and has demonstrated promising potential as a natural inhibitor [18]. Nevertheless, the effect of *S. crispus* leaf extract in corrosion inhibition upon aluminium in different pH ranges has not yet been investigated. The potential of *S. crispus* extract as an inhibitor is attributed to its active moieties, including flavonoids, phenolic acids, alkaloids, and ester glycosides that interact with metal surfaces to reduce corrosion rates [19]. Different reports on *S. crispus* extract have confirmed the presence of these moieties, which are known to facilitate metal complexation and oxide layer formation, thereby enhancing corrosion resistance [20]. Despite these advances, critical gaps remain in understanding the full potential of *S. crispus* as a corrosion inhibitor. While its corrosion inhibitors, such as flavonoids, phenolic acids, and alkaloids, have been studied for their medicinal properties, their corrosion inhibition mechanisms on aluminium across different pH conditions remain unexplored. Most existing research has focused on acidic environments, leaving a significant knowledge gap regarding its performance in neutral and alkaline media. Furthermore, the specific interactions between *S. crispus* phytochemicals and aluminium surfaces and the long-term stability of the protective layers they form require deeper investigation. This study aims to bridge these gaps by evaluating the corrosion inhibition efficiency of *S. crispus* leaf extract on aluminium in varying pH environments. We assess the extract's protective effects at different concentrations using weight loss measurements, electrochemical techniques, and surface characterization methods. By clarifying the relationship between *S. crispus* leaf extract's chemical composition and its corrosion inhibition performance, this work advances the development of sustainable, plant-based inhibitors while reducing reliance on hazardous synthetic compounds.

■ EXPERIMENTAL SECTION

Materials

Dried *S. crispus* leaves were purchased from Ten Organic Co., while methanol (CH_3OH) 99.5%, hydrochloric acid (HCl) 36%, sodium hydroxide (NaOH), and sodium chloride (NaCl) were purchased from Merck. Aluminum alloy substrates (dimensions: 10 × 50 × 3 mm) with a mass composition of 91% Al, 5.21% C, and 3.62% O were polished and used for corrosion testing.

Instrumentation

The extraction of *S. crispus* leaves was conducted using a Soxhlet apparatus. For structural characterization, the functional groups of the extract were identified by Fourier transform infrared spectroscopy (FTIR, PerkinElmer Spectrum 100). The FTIR samples were prepared as KBr pellets using a hydraulic press. Electrochemical measurements (Tafel polarization and EIS) were performed with an AUTOLAB PGSTAT30 potentiostat (Metrohm), and the surface morphology of the aluminum substrates was analyzed by scanning electron microscopy (SEM, JEOL JSM7800F).

Procedure

Crude leave extraction

As much as 20 g of ground leaves powder were placed in the cellulose thimble of the Soxhlet extractor, and around 300 mL of methanol was used to dissolve the extract. The process was performed at 67 °C for 12 h, then cooled to room temperature and filtered through Whatman filter paper (No. 1) in a filter funnel. The extracted biomaterial was dehydrated using a freeze-dryer.

Structural characterization

FTIR analysis was employed to uncover the chemical functional groups of the extract [21-22]. The typical testing procedure was as follows: 1 mg of the powder was mixed with 9 mg of KBr and ground until homogenized. The powder was pressed using a hydraulic press at 5 tons for 1 min to form a pellet, which was placed in the sample chamber. Characterization was performed in the range of 500 to 4500 cm^{-1} at a resolution of 4 cm^{-1} using a pure KBr pellet as background reference.

Corrosion inhibition studies

The weight loss and electrochemical corrosion investigations were performed in different pH including acidic HCl (pH 2), neutral NaCl (pH 7), and basic NaOH

(pH 10) solutions in different *S. crispus* extract concentrations of 0, 0.2, and 0.8 mg/L of the *S. crispus* extract. All the electrolytes were used from analytical grade chemical reagents in DI water without any purification.

Weight loss measurements. The aluminium sheets of 10 × 50 × 3 mm dimensions were polished with silicon carbide sandpapers of progressively finer grits: 400, 800, 1200, and finally 2000 grit. After each polishing stage, the samples were thoroughly rinsed with deionized water to remove surface debris, cleaned with acetone, dried, and kept from humidity [23]. Before immersion in the previously prepared solutions, the weight for each sample was recorded using an accurate digital balance. After 5, 10, 15, and 20 d of exposure, the specimens were taken out, rinsed thoroughly with DI water, dried, and weighed accurately again following the ASTM G1-03 for preparing, cleaning, and evaluation [24]. Three parallel experiments were performed for each test. The average weight loss, the corrosion rate, and the corrosion retention percentage were calculated using Eq. (1-3) [25-27]:

$$\Delta W = W1 - W2 \quad (1)$$

$$K = \frac{\Delta W}{st} \quad (2)$$

$$\eta_W = \frac{K_{zero} - K_{inh}}{K_{zero}} \times 100\% \quad (3)$$

where ΔW is the average weight of specimens before and after immersion exposure, K is the corrosion rate, s is the surface area in cm^2, t is the exposure time in days, η_W is the corrosion protection percentage, K_{zero} is the corrosion rate without an inhibitor, and K_{inh} is the corrosion rate with an inhibitor. Each sample's value is the mean value of three replicates.

Electrochemical measurements. Corrosion inhibition of the extract was determined at different pH values (2, 7, 10) using different electrolytes by investigating the electrochemical behavioral changes: without inhibitor, 0.2 mg/L inhibitor, and 0.8 mg/L inhibitor. Linear polarization curve (Tafel) and electrochemical impedance spectroscopy (EIS) were performed using (AUTOLAB PGSTAT30, Metrohm) under static conditions and in a three-electrode system; the reference electrode (Ag/AgCl), the counter electrode (Platinum wire), and an aluminium substrate as a working electrode. Experiments were performed after the immersion of the working electrode for 30 min before testing to maintain a steady state open circuit potential (E_{OCP}). After the E_{OCP} was stable, the EIS and Tafel were performed. Tafel curves were obtained in the potential range from ±250 mV with a 0.5 mV s^{-1} scan rate. From these curves, we extracted the anodic (β_a) and cathodic (β_c) slopes, which reveal whether the inhibitor affects the metal dissolution reaction or the hydrogen evolution reaction more strongly [28-29]. The corrosion current density (I_{corr}) obtained from the Tafel analysis was converted to actual corrosion rate using the standard conversion factor of 3.27×10^{-3}, which comes from unit conversions (millimeters per year, faraday constant, and density terms) that allow engineers to interpret the degradation rate in practical, real-world terms [2]. For the EIS measurements, a 10 mV AC signal was applied across a wide frequency range from 0.01 Hz down to 100 kHz. The resulting Nyquist plots showed semicircular shapes where larger diameters indicated better corrosion protection, while the accompanying Bode modulus plots helped confirm whether the inhibitor was forming a stable protective layer on the metal surface [30]. These impedance measurements are crucial for revealing how strongly and effectively the inhibitor molecules adsorb onto the aluminum, which can't be fully understood from Tafel analysis alone [1]. By combining both Tafel and EIS methods, a comprehensive understanding of electrochemical behavior can be established. This dual approach is essential for developing effective corrosion inhibitors in real-world performance, which depends on both chemical and physical protection mechanisms working together. The entire test was performed under static conditions to simulate environmental stresses. This methodology provides reliable data that can be directly applied to industrial corrosion prevention strategies.

Surface morphology study

The surface morphology of the aluminium samples was observed after exposure to electrolytes in the presence of 0.2 mg/L *S. crispus* extract and in the absence

of the extract. The surface morphology changes upon using an inhibitor, confirmed by employing SEM.

■ RESULTS AND DISCUSSION

FTIR Analysis of *Strobilanthes crispus* Extract

The FTIR spectrum of *S. crispus* extract in Fig. 1 revealed key functional groups including hydroxyl/amine (O–H/N–H), carbonyl (C=O), ether/alcohol (C–O), metal-oxygen (M–O), and alkyl/alkene (C–H) that play an important role in the protective oxide film formation, potentially contributing to corrosion inhibition. All peaks and their corresponding functional groups were tabulated in Table 1. The broad peak observed near 3200–3600 cm^{-1} is related to O–H/N–H stretching, indicating the presence of organic amines and alcohols, which can facilitate metal ion chelation and oxide formation. The peak at 2850 cm^{-1} is attributed to C–H stretching, confirming the presence of organic compounds. Additionally, the characteristic stretching at 1732 cm^{-1} suggests the presence of C=O groups, which can serve as active sites for metal complexation [21-22]. The intense absorption band around 1142–1341 cm^{-1} may be associated with C–O stretching, which can also serve as active sites for metal complexation [31]. Furthermore, the fingerprint region below 950 cm^{-1} exhibits peaks characteristic of M–O vibrations (500–800 cm^{-1}), which may be attributed to ZnO, Al_2O_3, and CuO [32]. These oxides likely originated through two primary pathways: first, the complexation of

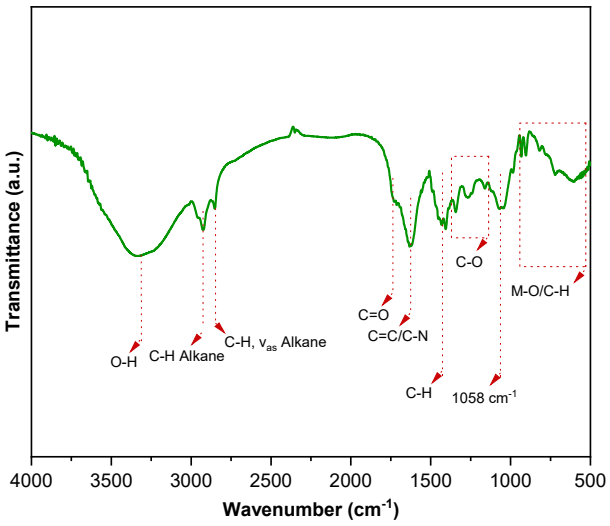

Fig 1. FTIR spectrum for *S. crispus* extract

Table 1. Infrared transmission on several functional groups of *S. crispus* leaf extract

Wavenumber (cm^{-1})	Spectrum interpretation
559–951	M–O/C–H alkenes
1058	C–O–C of polysaccharide/alcohol
1142–1341	C–O
1430	C–H
1625	C=C/C–N
1732	C=O
2850	C–H alkane
2930	C–H alkane
3200–3600	O–H

trace metal ions including Zn^{2+} and Cu^{2+} naturally present in the plant biomass by bioactive compounds like flavonoids and phenolic acids, which subsequently oxidize upon interaction with the aluminium substrate [33]; second, the direct oxidation of Al^{3+} ions released from the substrate in alkaline media, forming a passive Al_2O_3 layer [34]. These oxides are known for passive layer formation on the metal interface, enhancing corrosion resistance. The presence of these functional groups suggests that the extract facilitates metal oxide deposition, forming a protective barrier that limits oxygen and moisture diffusion, thereby mitigating corrosion. The findings confirm that *S. crispus* extract acts as a potential green corrosion inhibitor by promoting organic molecule adsorption and forming stable oxide layers, particularly ZnO, SiO_2, Al_2O_3, and CuO, which contribute to enhanced material protection.

Corrosion Inhibition Evaluation

Weight loss method

The K value on the aluminium substrate after 20 d of immersion in HCl (pH 2), NaCl (pH 7), and NaOH (pH 10) electrolytes in the presence and absence of inhibitors at different concentrations was calculated following Eq. (2) and the data are presented in Fig. 2. In acidic, basic, and neutral electrolytes, the inhibitor showed a decline in corrosion rate over time compared with the absence of an inhibitor, which indicates the wide spectrum of corrosion inhibition at the anodic and cathodic regions. The blank tests (0 inhibitor) revealed expected trends: aluminium corroded fastest in HCl (pH 2) due to H^+ driven dissolution, while NaOH (pH 10) promoted

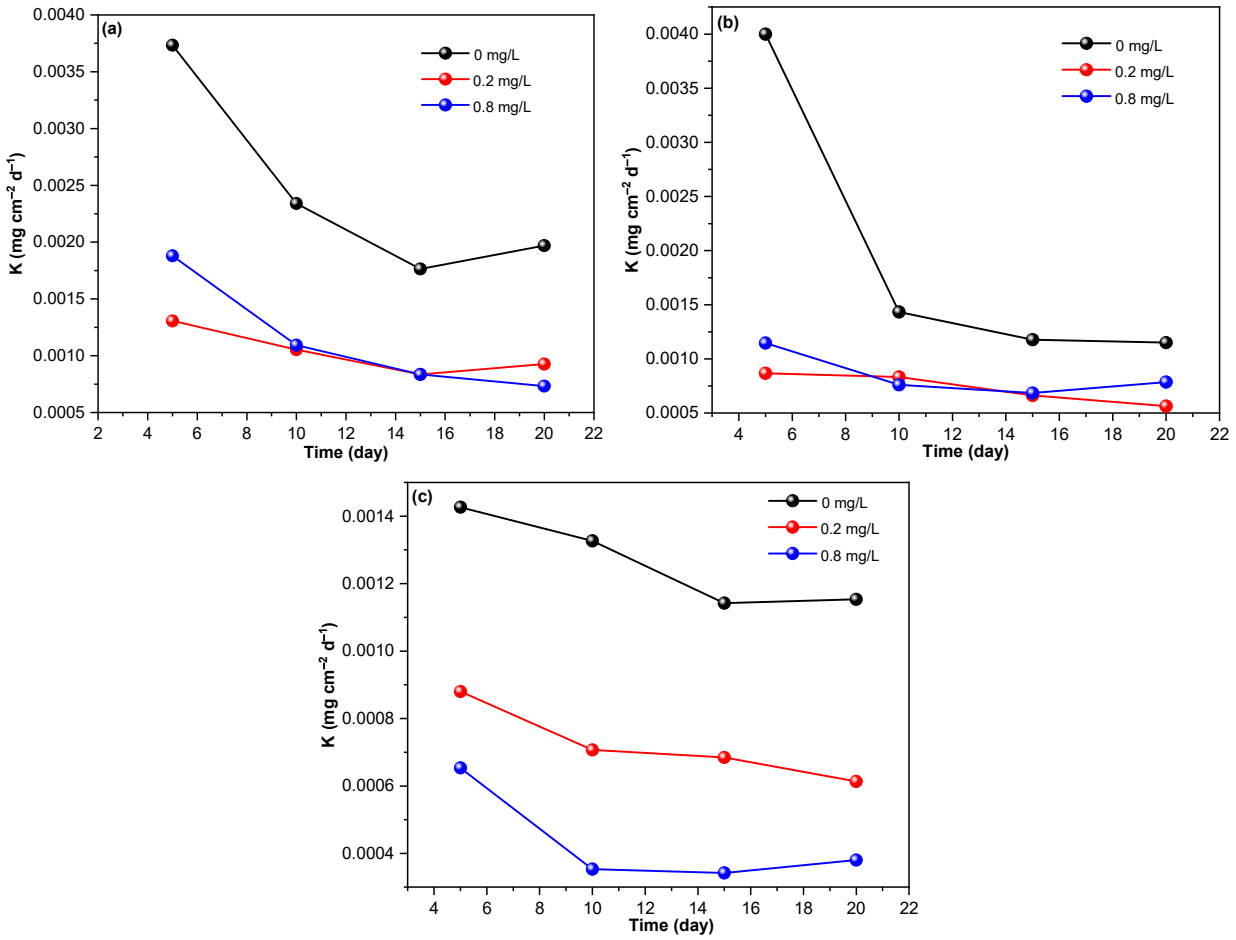

Fig 2. Relationship between the corrosion rate and inhibitor concentration for aluminum after 20 d of immersion in (a) HCl, (b) NaCl, and (c) NaOH at 25 °C

passivation via Al_2O_3 formation. NaCl (pH 7) showed intermediate rates, as Cl^- ions induced pitting despite neutral pH. Notably, the inhibitor reduced corrosion rates across all conditions, with the most pronounced effect in alkaline media (75.5% efficiency in NaOH), where its organic components synergized with the native oxide layer. Further, the increase in the inhibitor concentration directly impacts decreasing the corrosion rate in all electrolytes, which could be attributed to the accumulation of oxide film in the aluminium interface, preventing corrosive ions from reaching the active aluminium layer. After 20 d of immersion in NaOH electrolyte, the corrosion rate was recorded as 0.00061 and 0.00038 mm/y in the presence of 0.2 and 0.8 mg/L of inhibitor, respectively. In neutral and acidic electrolytes, however, the inhibitor concentration has no significant effect on corrosion inhibition. The same trend can be confirmed by investigating the corrosion reduction percentage (η_W) in Fig. 3, where the corrosion reduction percentage in NaOH after 20 d of immersion was recorded as 46.8 and 67.05% in immersion with 0.2 and 0.8 mg/L of inhibitor, respectively. It is worth mentioning that the highest corrosion reduction percentage recorded after ten days of immersion in NaOH was about 75.5% in the presence of 0.8 mg/L inhibitor. The results confirm the very good effect of the extract at the same concentration and exposure time on corrosion inhibition of aluminium in a harsh environment of NaOH than in acidic or neutral environments, which competes with other plant extract inhibitors as presented in Table 3.

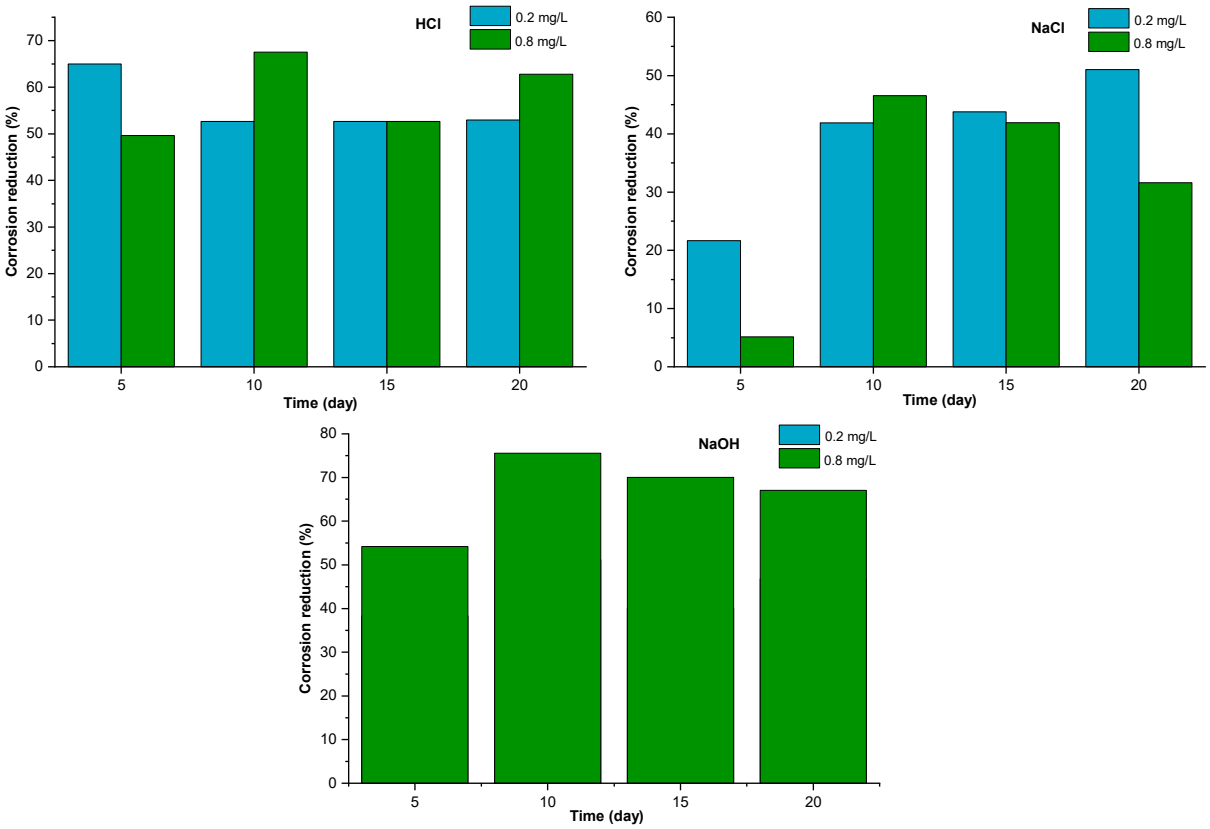

Fig 3. The bar chart shows the effect of immersion time on corrosion reduction percentage in different *S. crispus* extract concentrations at different electrolytes

Polarization curve (Tafel)

Evaluating corrosion resistance helps determine a material's durability and lifetime. Among various techniques used to assess corrosion performance, Tafel polarization curves are widely employed for quantitative and qualitative analysis via different parameters. To investigate different effects of corrosion inhibition at different *S. crispus* extract concentrations, the dynamic polarization of Al-substrates was evaluated after 20 d of exposure in HCL, NaCl, and NaOH electrolytes, as shown in Fig. 4. The electrochemical parameters, including corrosion potential (E_{corr}), corrosion current density (I_{corr}), anode Tafel slope (β_a), cathode Tafel slope (β_c), and corrosion rate (CR) obtained from the polarization curve are presented in Table 2. After 20 d of immersion in NaOH and in the presence of inhibitor at different concentrations, the E_{corr} shifted toward the positive region, indicating that the synthesized inhibitor at different concentrations has an advanced corrosion inhibition effect compared to the absence of an inhibitor. It is worth mentioning that inhibitors at different concentrations were able to shift the E_{corr} toward a more positive region only in NaOH, while shifting toward the more negative region in HCl and NaCl electrolytes [1]. Further, the CR of the aluminium in NaOH elucidates the lowest value of about 0.00022 mm/y compared to the absence of inhibitor, the CR value recorded as 0.019 mm/y. The anodic and cathode slops sloping branches in 0.2 mg/L were 65.24 and 116.08 mV/dec, which are lower than the immersed substrate in zero mg/L *S. crispus* inhibitor. The results show that the presence of inhibitor at different concentrations has better corrosion inhibition compared with the absence of inhibitor in NaOH, meaning carbonaceous compounds, including C–O and C=O can be adsorbed on the aluminium interface and chemically react with Al or its ions. At the same time, M–O can be involved in the adsorption of oxygen moieties and reduce the cathodic reaction [13-14]. As is known, the oxide

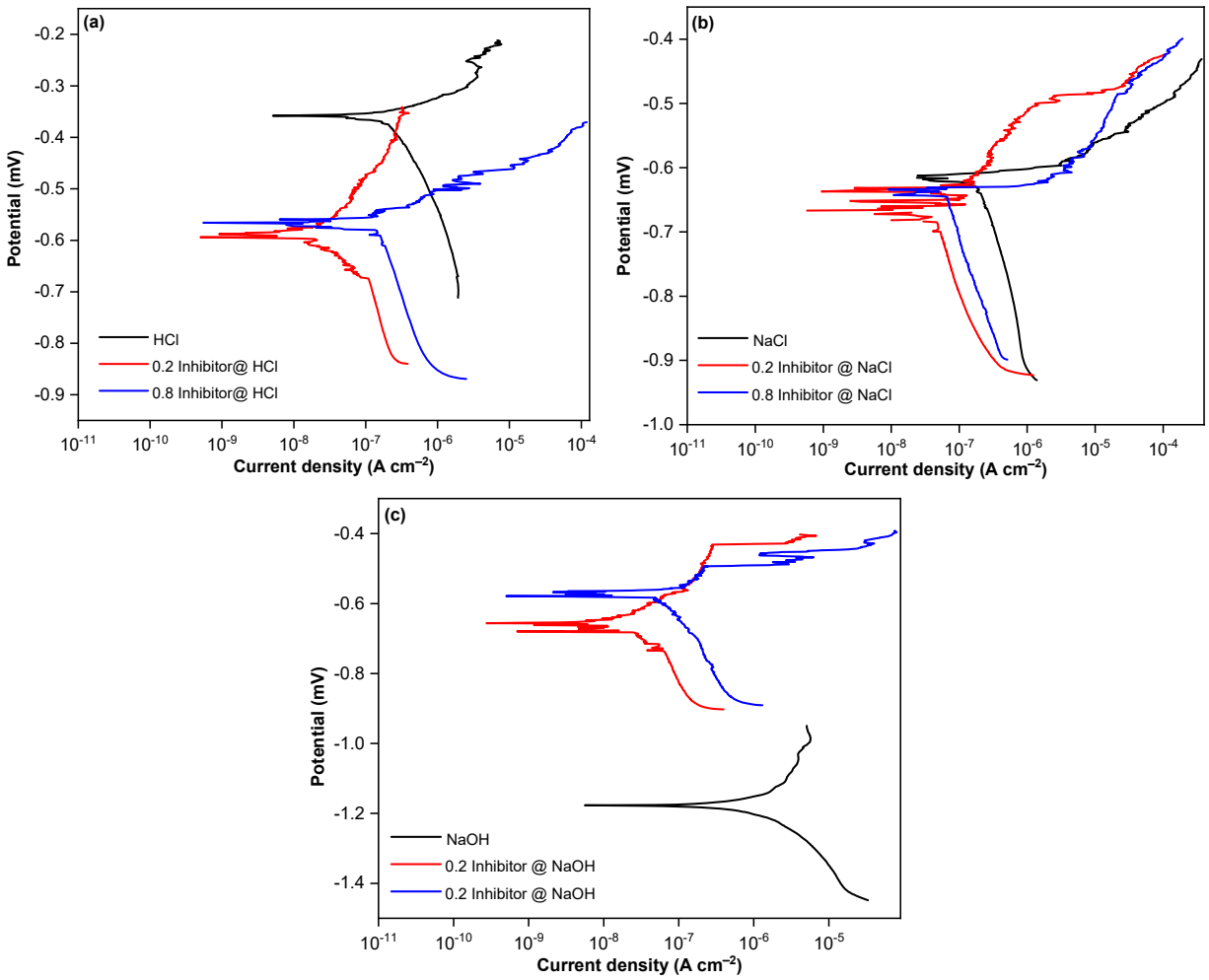

Fig 4. Polarization plots of aluminum after 20 d of immersion in (a) HCl, (b), NaCl, and (c) NaOH with different inhibitor concentrations

Table 2. Tafel polarization parameters after 20 d of exposure to different *S. crispus* inhibitor concentrations and electrolytes

Inhibitor (mg/L)	Electrolyte	E_{corr} (V)	I_{corr} (mA/cm^2)	β_a (mV/dec)	$-\beta_c$ (mV/dec)	η_W	CR (mm/y)
0	HCl	−0.4000	0.0024	171.4800	86.6900	-	0.02900
0.2	HCl	−0.0580	0.3230	804.8500	719.0500	52.9600	0.00370
0.8	HCl	−0.5700	0.0440	11.7700	31.9100	62.7700	0.00050
0	NaCl	−0.6400	0.4090	95.7600	44.4100	-	0.00400
0.2	NaCl	−0.6700	0.0310	24.4900	70.9200	51.0100	0.00030
0.8	NaCl	−0.6600	0.2110	63.1400	40.6900	31.5900	0.00240
0	NaOH	−1.1000	0.00170	103.9100	102.8200	-	0.01900
0.2	NaOH	−0.6500	0.0190	65.2400	116.0800	46.8200	0.00022
0.8	NaOH	−0.5900	0.1960	775.9400	82.2100	67.0500	0.00022

status of M–O possesses a great corrosion inhibition effect on the cathodic reactions. Hence, the synthesized oxide layer directly inhibited the corrosion reaction in the anodic region, as confirmed by the low I_{corr} of the Al substrate with the inhibitor in the NaOH electrolyte. Table 3 compares the corrosion rate results of this report

Table 3. Comparison of *S. crispus* extract results with other extract inhibitors in acid solutions

Plant extract	Concentration	Substrate	Electrolyte	CR (mm/y)	η_W (%)	Reference
Maple	0.4 g/L	A1010 LCS	1 M HCl	0.116	93.0	[35]
Pisum sativum peel	0.4 g/L	MS	1 M HCl	0.349	90.0	[36]
Ruellia tuberosa L	1.2 g/L	Copper	0.5 M HCl	0.0059	87.0	[36]
Aesculus hippocastanum	140 mg/L	Copper alloy	3 m H_3PO_4	1.460	96.1	[37]
Palm oil leaves	0.6 g/L	CS	3.5% NaCl	0.090	N/A	[38]
Carmichaelii Debx extract	200 mg/L	Q235 CS	1 M HCl	0.003	98.0	[39]
Strobilanthes crispus	0.4 mg/L	Al-substrate	1 M NaOH	0.00022	75.5	This work

with those from previous studies, highlighting its competitive performance.

Electrochemical impedance spectroscopy (EIS)

The EIS technique was used to study the effectiveness of the inhibitor at different concentrations in preventing corrosive ions from reaching the metal substrate after 20 d of immersion at different pH. The results were expressed as Nyquist and Bode plots, as presented in Fig. 5. The Nyquist plots (Fig. 5(a-c)) exhibited two distinct semicircles, representing the charge transfer resistance (R_{ct}) at high frequencies and the oxide film resistance (R_{of}) at low frequencies. The larger semicircle diameter in NaOH (0.8 mg/L inhibitor) indicates superior corrosion resistance, corroborated by the highest R_{ct} value of $6.80 \times 10^4\ \Omega$ (Table 4). This suggests the formation of a dense protective layer, likely due to synergistic interactions between phytochemicals and the aluminium surface. The Bode modulus plots (Fig. 5(d–f)) further confirmed this, with a phase angle shift toward higher frequencies, indicative of stable film formation. These results align with prior studies on plant-derived inhibitors, where high R_{ct} values correlate with effective adsorption and barrier properties [40-41]. It is worth mentioning that the inhibitor concentration of 0.8 mg/L elucidated the highest impedance arc and modulus at the med/high-frequency regions under basic conditions, indicating that the corrosion resistance of the inhibitor works better than that of other environments. The fitted models of the equivalent circuit (EEC) in free-inhibitor and with inhibitor were illustrated in Fig. 6(a–b), which showed the fitting analysis of the impedance spectra of the electrolyte/electrode in model a, while it shows the electrolyte/oxide film/substrate system in model b. The models are composed of five possible circuit components, namely, R_s is electrolyte resistance, R_{ct} is the charge transfer resistance, R_{of} is the oxide film resistance, CPE_c is the constant phase element for coating replacing the ideal capacitance due to the metal interface dispersion, and W_s is the Warburg impedance generated by ion diffusion of some corrosion products through coating matrix.

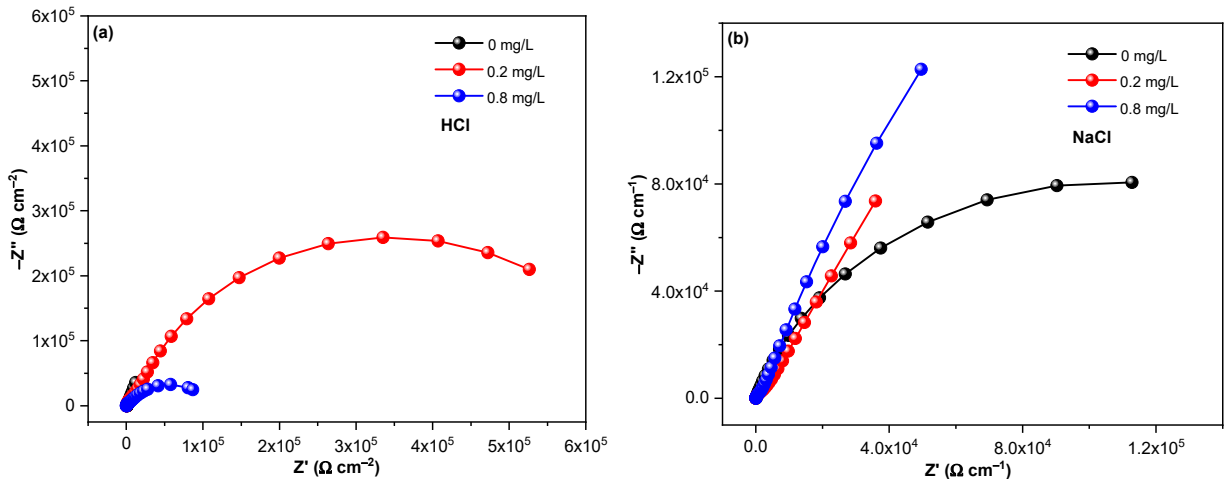

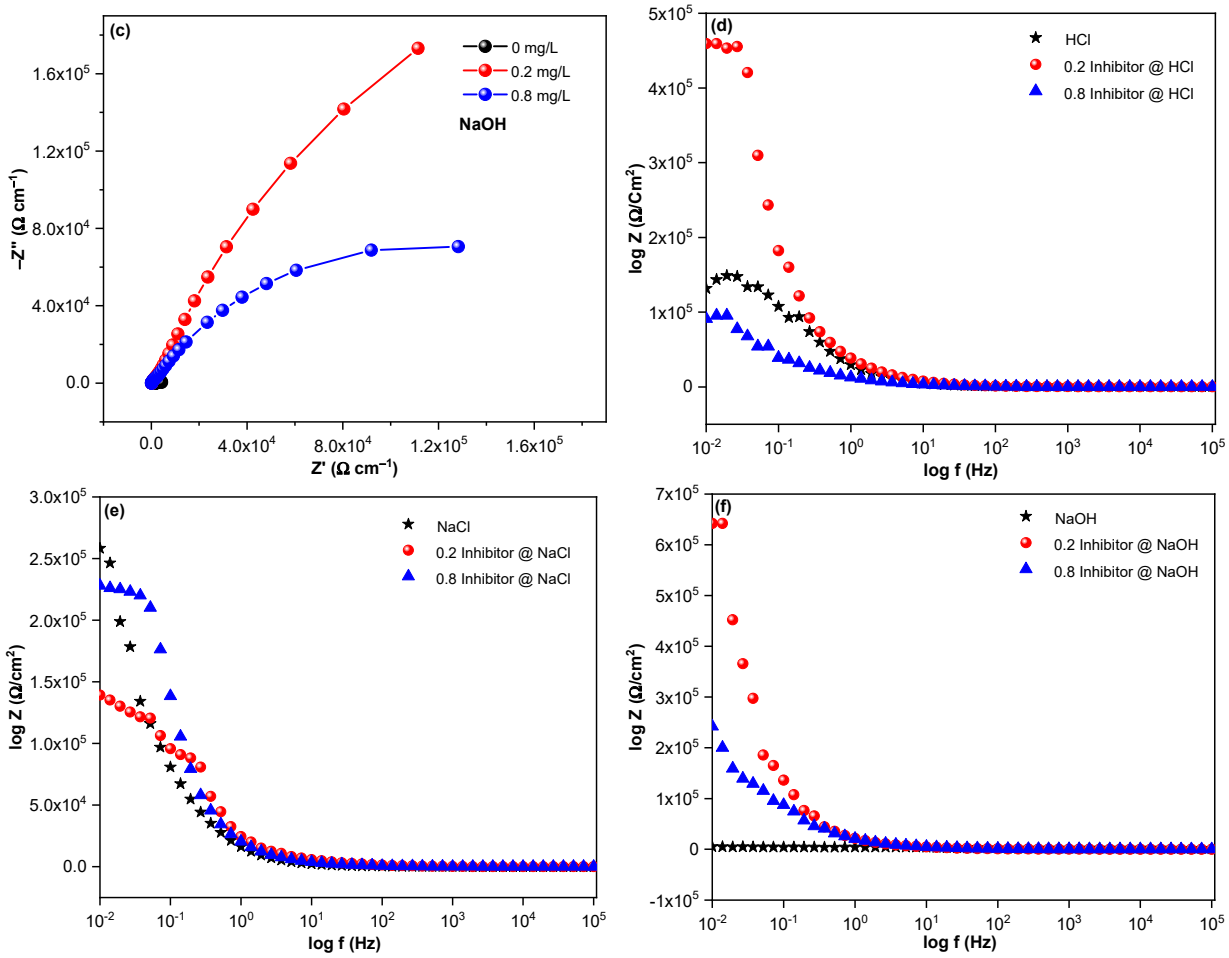

Fig 5. Nyquist plot at different *S. crispus* extract concentrations for aluminum in (a) HCl, (b) NaCl, and (c) NaOH. Bode plot at different *S. crispus* extract concentrations for aluminum in (d) HCl, (e) NaCl, and (f) NaOH

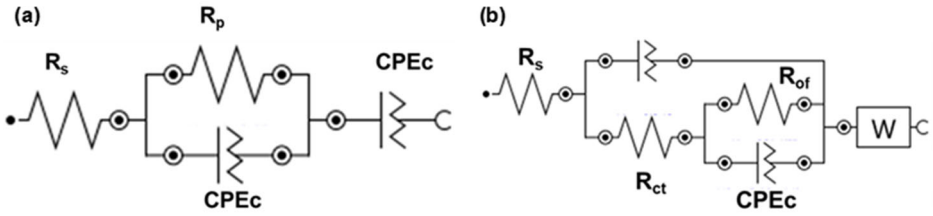

Fig 6. Fitted circuit models: (a) without inhibitor and (b) with inhibitor

The parameters obtained by EEC's fitting impedance are tabulated in Table 4. Compared with the electrolyte without an inhibitor, the R_s, R_{ct}, and R_{of} are significantly improved with inhibitor interference. On the one hand, it indicates that with the participation of an inhibitor, the metal interface may form a dense protective oxide barrier. On the other hand, it confirms that in the cathode region, the released M^+ ions from the metal oxide content adsorb oxygen molecules and deposit on the active surface of the Al-substrate. Further, carbonyl and carboxyl groups in the anodic region react with Al or Al^{3+} to form organic-inorganic complexes, which provides another piece of evidence that both anodic and cathodic reactions were slowed down, as also confirmed previously by the dynamic potential polarization study [42]. Consequently, these findings underline the importance of carefully adjusting the inhibitor concentration to achieve optimal protective characteristics. In the Bode

Table 4. Fitter circuits parameters

Electrolyte	Inhibitor concentration (mg/L)	R_s (Ω)	R_{ct} (Ω)	R_{of} (Ω)	CPE_c (Ω^{-1} cm^{-2} s)	W_s (Ω cm^{-2})
HCl	0.0	2.66×10^5	6.45×10^5	-	10.18	
	0.2	2.49×10^5	0.40×10^5	6.00×10^5	7.68	1.41×10^{-4}
	0.8	47.40	3.10×10^3	1.10×10^5	27.60	-
NaCl	0.0	35.30	2.15×10^5	-	15.50	-
	0.2	19.80	1.03×10^4	1.60×10^3	10.82	-
	0.8	11.50	7.17×10^4	2.10×10^3	10.82	
NaOH	0.0	314.00	5.00×10^3	-	7.61	-
	0.2	121.00	1.73×10^4	6.84×10^5	26.50	0.29×10^{-4}
	0.8	75.60	6.80×10^4	1.19×10^6	19.26	0.01×10^{-4}

modulus Fig. 5 (d, e, and f), the Bode modulus shifts toward high frequency in the presence of 0.2 mg/L inhibitor in HCl and NaOH. The phenomenon is thought to be strongly related to the formation of oxide film in the anodic and the cathodic regions [43]. Endowing inhibitors with the advancement of long-term workability [44].

Surface Study

To reveal the anticorrosive effect of *S. crispus* extract microscopically, aluminium substrates were immersed in a 1 M NaOH electrolyte with 0.8 mg/L *S. crispus* extract for 20 d, and then the interface changes were determined by SEM. From Fig. 7(a), the aluminium surface after immersion in an inhibitor-free medium was uneven and covered with lots of corrosion products, indicating that the aluminium sample was suffering from a severe corrosion state. The aluminium surface after immersion in NaOH with *S. crispus* extract in Fig. 7(b) was smoother and layered with a few corrosion products, which means that the corrosion of the sample is non-aggressive. This demonstrates the inhibitory action of *S. crispus* extract.

Inhibitive Mechanism of *S. crispus* Extract

From the previous results, the adsorptive mechanism of *S. crispus* extract on aluminum substrate can be proposed as an inhibitor-free medium, as illustrated in Fig. 8; corrosive ions could be deposited at the aluminum surface easily, causing serious corrosion of aluminum. Upon *S. crispus* extract incorporation, the main chemical compositions of *S. crispus* (such as metal ions, phenolics, and caffeine) were able to compete with other corrosive ions to be deposited on the aluminum surface through the N and O atoms by forming Al–N and Al–O bonds [45-47]. Therefore, the adsorbed *S. crispus* organic content can impede corrosive ions from reaching the aluminum interface, thereby retarding the corrosion of the substrate.

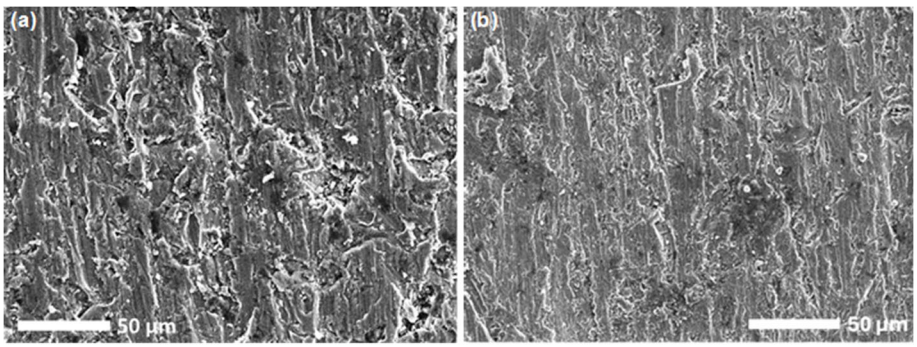

Fig 7. SEM image of the aluminum substrate after immersion for 20 d in (a) NaOH without inhibitor and (b) NaOH electrolyte with 0.8 mg/L inhibitor

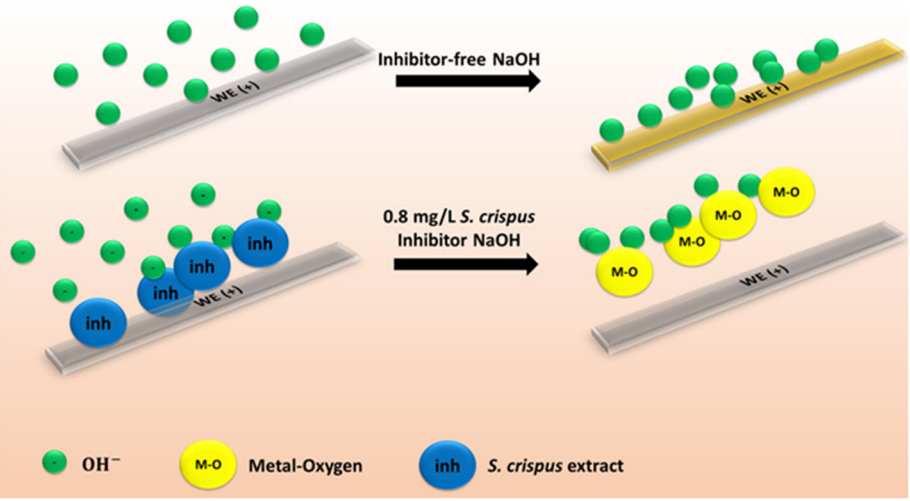

Fig 8. Schematic representation of the *S. crispus* inhibitor adsorption mechanism on the aluminum surface in 1 M NaOH solution

■ CONCLUSION

This study demonstrates that *S. crispus* extract is an effective, eco-friendly corrosion inhibitor for aluminium, with performance highly dependent on pH. Electrochemical and weight loss analyses revealed superior inhibition (75.5% efficiency) in alkaline conditions (pH 10) at a low concentration of 0.8 mg/L, facilitated by stable adsorption on the metal surface. Performance was moderate in acidic and neutral media due to competitive ion effects. These findings position the extract as a promising green alternative for alkaline environments. Future work should focus on enhancing its broad-spectrum efficacy through synergistic formulations and detailed mechanistic studies to confirm its long-term industrial applicability.

■ ACKNOWLEDGMENTS

The authors sincerely acknowledge the financial support provided by Universiti Malaysia Pahang Al-Sultan Abdullah, under Internal Research Grant No. RDU210350.

■ CONFLICT OF INTEREST

The authors declare that they have no known competing financial interests or personal relationships that could have appeared to influence the work reported in this paper.

■ AUTHOR CONTRIBUTIONS

All authors contributed equally to this work. They were involved in conceptualization, methodology, data curation, formal analysis, investigation, validation, resources, writing original draft, and writing review & editing. Additionally, all authors have read and approved the final manuscript.

■ REFERENCES

[1] Albarqouni, Y., Abu Bakar, N., Thalji, M.R., and Abdullah, A., 2025, Self-polymerization of dopamine on zinc oxide nanoparticles for enhanced corrosion resistance in epoxy-aluminum coatings, *Chin. J. Chem. Eng.*, 85, 304–315.

[2] Albarqouni, Y., Banius, E., Abu Bakar, N.H., and Abdullah, A., 2025, Enhancing epoxy coatings with spherical ZnO nanoparticles for improved hydrophobicity and corrosion resistance, *J. Adhes. Sci. Technol.*, 39 (19), 3009–3029.

[3] Izadi-Najafabadi, A., Yasuda, S., Kobashi, K., Yamada, T., Futaba, D.N., Hatori, H., Yumura, M., Iijima, S., and Hata, K., 2010, Extracting the full potential of single-walled carbon nanotubes as durable supercapacitor electrodes operable at 4 V with high power and energy density, *Adv. Mater.*, 22 (35), E235–E241.

[4] Obaid, H.T., Mutar, M.M., and Ali, S.H., 2025, Sulfasalazine as a corrosion inhibitor on carbon steel metal surfaces in acidic media using the hydrogen evolution method: Experimental and theoretical studies, *Indones. J. Chem.*, 25 (1), 90–99.

[5] Hadisaputra, S., Purwoko, A.A., and Hamdiani, S., 2022, Copper corrosion protection by 4-hydrocoumarin derivatives: insight from density functional theory, ab initio, and Monte Carlo simulation studies, *Indones. J. Chem.*, 22 (2), 413–428.

[6] Albarqouni, Y., Ali, G.A.M., Chong, F.C., Abu Bakar, N.H., Althobiti, R., and Abdullah, A., 2024, Recent advances of the ultimate microbial influenced corrosion (MIC): A review, *Curr. Nanosci.*, 20, 1–14.

[7] Ali, N., Fonna, S., Saputra, Y., Ariffin, A.K., and Supardi, J., 2025, Efficiency of *Syzygium cumini* fruit extract as a green corrosion inhibitor for low carbon steel in hydrochloric acid solution, *Indones. J. Chem.*, 25 (3), 823–836.

[8] Chaubey, N., Savita, S., Qurashi, A., Chauhan, D.S., and Quraishi, M.A., 2021, Frontiers and advances in green and sustainable inhibitors for corrosion applications: A critical review, *J. Mol. Liq.*, 321, 114385.

[9] Al Jahdaly, B.A., Maghraby, Y.R., Ibrahim, A.H., Shouier, K.R., Alturki, A.M., and El-Shabasy, R.M., 2022, Role of green chemistry in sustainable corrosion inhibition: A review on recent developments, *Mater. Today Sustainability*, 20, 100242.

[10] Pan, Y., Qin, R., Hou, M., Xue, J., Zhou, M., Xu, L., and Zhang, Y., 2022, The interactions of polyphenols with Fe and their application in Fenton/Fenton-like reactions, *Sep. Purif. Technol.*, 300, 121831.

[11] M'hiri, N., Veys-Renaux, D., Rocca, E., Ioannou, I., Boudhrioua, N.M., and Ghoul, M., 2016, Corrosion inhibition of carbon steel in acidic medium by orange peel extract and its main antioxidant compounds, *Corros. Sci.*, 102, 55–62.

[12] Wang, J., Hou, B., Xiang, J., Chen, X., Gu, T., and Liu, H., 2019, The performance and mechanism of bifunctional biocide sodium pyrithione against sulfate reducing bacteria in X80 carbon steel corrosion, *Corros. Sci.*, 150, 296–308.

[13] Zgueni, H., El Mesky, M., Moussaif, A., Salah, M., Matine, A., Oubair, A., Znini, M., Mabrouk, E.H., Echihi, S., and Chebabe, D., 2025, Theoretical and experimental study of the corrosion inhibition of carbon steel in 1M HCl solution by a new synthesized organic compound derived from carbendazim, *J. Mol. Struct.*, 1327, 141230.

[14] Wysocka, J., Cieslik, M., Krakowiak, S., and Ryl, J., 2018, Carboxylic acids as efficient corrosion inhibitors of aluminium alloys in alkaline media, *Electrochim. Acta*, 289, 175–192.

[15] Mungwari, C.P., Obadele, B.A., and King'ondu, C.K., 2025, Phytochemicals as green and sustainable corrosion inhibitors for mild steel and aluminium: Review, *Results Surf. Interfaces*, 18, 100374.

[16] Koh, R.Y., Lim, F.P., Ling, L.S.Y., Ng, C.P.L., Liew, S.F., Yew, M.Y., Tiong, Y.L., Ling, A.P.K., Chye, S.M., and Ng, K.Y., 2017, Anticancer mechanisms of *Strobilanthes crispa* Blume hexane extract on liver and breast cancer cell lines, *Oncol. Lett.*, 14 (4), 4957–4964.

[17] Badawy, I., Darwish, M.K., Samir, O., Baraqouni, Y., Nassef, M.M., Elshafey, H.E., Mahmoud, S.M., and El Deeb, H.H., 2015, RECK gene polymorphisms in hepatocellular carcinoma and cirrhotic patients related to hepatitis C virus, *Donnish J. Biomed. Res.*, 2 (1), 1–6.

[18] Yaacob, N.S., Hamzah, N., Nik Mohamed Kamal, N.N., Zainal Abidin, S.A., Lai, C.S., Navaratnam, V., and Norazmi, M.N., 2010, Anticancer activity of a sub-fraction of dichloromethane extract of *Strobilanthes crispus* on human breast and prostate cancer cells *in vitro*, *BMC Complementary Altern. Med.*, 10 (1), 42.

[19] Ng, M.G., Ng, C.H., Ng, K.Y., Chye, S.M., Ling, A.P.K., and Koh, R.Y., 2021, Anticancer properties of *Strobilanthes crispus*: A review, *Processes*, 9 (8), 1370.

[20] Chen, C.S., Tan, S.P., Loke, C.F., and Poh, T.V., 2023, Traditional uses, phytochemistry and pharmacological properties of *Strobilanthes crispa* (L.) Blume., *Rec. Nat. Prod.*, 17 (5), 743–792.

[21] Albarqouni, Y.M.Y., Lee, S.P., Ali, G.A.M., Ethiraj,

A.S., Algarni, H., and Chong, K.F., 2022, Facile synthesis of reduced graphene oxide aerogel in soft drink as supercapacitor electrode, *J. Nanostruct. Chem.*, 12 (3), 417–427.

[22] Albarqouni, Y., Ali, G.A.M., Lee, S.P., Mohd-Hairul, A.R., Algarni, H., and Chong, K.F., 2021, Dual-functional single stranded deoxyribonucleic acid for graphene oxide reduction and charge storage enhancement, *Electrochim. Acta*, 399, 139366.

[23] El Ibrahimi, B., and Berdimurodov, E., 2023, "Weight Loss Technique for Corrosion Measurements" in *Electrochemical and Analytical Techniques for Sustainable Corrosion Monitoring*, Elsevier, Amsterdam, Netherlands, 81–90.

[24] Ali, S.I., and Ahmad, S.N., 2023, Tribo-corrosion behavior of Zn-Ni-Cu and Zn-Ni-Cu-TiB_2 coated mild steel, *Arabian J. Chem.*, 16 (5), 104648.

[25] Hossain, N., Chowdhury, M.A., Rana, M., Hassan, M., and Islam, S., 2022, *Terminalia arjuna* leaves extract as green corrosion inhibitor for mild steel in HCl solution, *Results Eng.*, 14, 100438.

[26] Pyun, S.I., and Moon, S.M., 2000, Corrosion mechanism of pure aluminium in aqueous alkaline solution, *J. Solid State Electrochem.*, 4 (5), 267–272.

[27] Ashassi-Sorkhabi, H., Mirzaee, S., Rostamikia, T., and Bagheri, R., 2015, Pomegranate (*Punica granatum*) peel extract as a green corrosion inhibitor for mild steel in hydrochloric acid solution, *Int. J. Corros.*, 2015 (1), 197587.

[28] Milošev, I., 2024, Corrosion inhibition of aluminium alloys by molybdate ions: A critical review of the chemistry, mechanisms and applications, *Corros. Sci.*, 229, 111854.

[29] Lin, G., Zheng, Y., Bian, S., Lian, Y., Chen, Y., Lv, J., and Huang, B., 2024, Improving the performance of geopolymer-based wood adhesives using a green mechanochemical strategy, *Int. J. Adhes. Adhes.*, 129, 103558.

[30] Lazanas, A.C., and Prodromidis, M.I., 2023, Electrochemical impedance spectroscopy—A tutorial, *ACS Meas. Sci. Au*, 3 (3), 162–193.

[31] Ch'ng, Y.S., Tan, C.S., Loh, Y.C., Ahmad, M., Asmawi, M.Z., and Yam, M.F., 2016, Vasorelaxation study and tri-step infrared spectroscopy analysis of Malaysian local herbs, *J. Pharmacopunct.*, 19 (2), 145–154.

[32] Suboh, S.F., Mahat, A.M., Yusof, M.H., and Wan Abdul Razak, W.R., 2022, Antimicrobial activity of *Strobilanthes crispus* leaves aqueous extract and green biosynthesis iron oxide nanoparticles against selected human pathogens, *Asia-Pac. J. Mol. Biol. Biotechnol.*, 30 (4), 20–32.

[33] Hu, Q., Lou, M., Wang, R., Bai, S., Guo, H., Zhou, J., Ma, Q., Wang, T., Zhu, L., and Zhang, X., 2024, Complexation with metal ions affects chlorination reactivity of dissolved organic matter: Structural reactomics of emerging disinfection byproducts, *Environ. Sci. Technol.*, 58 (31), 13890–13903.

[34] Wang, R., Li, P., Zhou, W., Li, Y., Gao, K., and Ouyang, Y., 2024, Study on oxidation mechanism of aluminum surface under applied electric field, *Mater. Chem. Phys.*, 318, 129224.

[35] Jokar, M., Farahani, T.S., and Ramezanzadeh, B., 2016, Electrochemical and surface characterizations of *Morus alba* Pendula leaves extract (MAPLE) as a green corrosion inhibitor for steel in 1M HCl, *J. Taiwan Inst. Chem. Eng.*, 63, 436–452.

[36] Srivastava, M., Tiwari, P., Srivastava, S.K., Kumar, A., Ji, G., and Prakash, R., 2018, Low cost aqueous extract of *Pisum sativum* peels for inhibition of mild steel corrosion, *J. Mol. Liq.*, 254, 357–368.

[37] Deyab, M.A., Mohsen, Q., and Guo, L., 2022, *Aesculus hippocastanum* seeds extract as eco-friendly corrosion inhibitor for desalination plants: Experimental and theoretical studies, *J. Mol. Liq.*, 361, 119594.

[38] Abdullah, A., Banius, E., Sofian, A.H., and Bin, L.W., 2023, "Evaluation of Palm Oil Leaves Extracts as a Potential Environment Friendly Corrosion Inhibitor for Metals" in *Proceedings of the 2nd Energy Security and Chemical Engineering Congress*, Eds. Johari, N.H., Wan Hamzah, W.A., Ghazali, M.F., Setiabudi, H.D., and Kumarasamy, S., Springer Nature, Singapore, 387–399.

[39] Xu, N., Yang, X.B., and Zhang, Q.H., 2024, Insight into interfacial adsorption and inhibition

mechanism of *Aconitum carmichaelii* Debx extract as high-efficient corrosion inhibitor for carbon steel in acidic solution, *J. Mol. Liq.*, 39, 123602.

[40] Ramezanzadeh, B., Bahlakeh, G., and Ramezanzadeh, M., 2018, Polyaniline-cerium oxide (PAni-CeO_2) coated graphene oxide for enhancement of epoxy coating corrosion protection performance on mild steel, *Corros. Sci.*, 137, 111–126.

[41] Xia, N.N., Xiong, X.M., Wang, J., Rong, M.Z., and Zhang, M.Q., 2016, A seawater triggered dynamic coordinate bond and its application for underwater self-healing and reclaiming of lipophilic polymer, *Chem. Sci.*, 7 (4), 2736–2742.

[42] Najmi, P., Keshmiri, N., Ramezanzadeh, M., and Ramezanzadeh, B., 2021, Synthesis and application of Zn-doped polyaniline modified multi-walled carbon nanotubes as stimuli-responsive nanocarrier in the epoxy matrix for achieving excellent barrier-self-healing corrosion protection potency, *Chem. Eng. J.*, 412, 128637.

[43] Jain, D., Pareek, S., Agarwala, A., Shrivastava, R., Sassi, W., Parida, S.K., and Behera, D., 2021, Effect of exposure time on corrosion behavior of zinc-alloy in simulated body fluid solution: Electrochemical and surface investigation, *J. Mater. Res. Technol.*, 10, 738–751.

[44] Qian, B., Zheng, Z., Michailids, M., Fleck, N., Bilton, M., Song, Y., Li, G., and Shchukin, D., 2019, Mussel-inspired self-healing coatings based on polydopamine-coated nanocontainers for corrosion protection, *ACS Appl. Mater. Interfaces*, 11 (10), 10283–10291.

[45] Jayakumar, S., Jouhar, M., Khan, F., Vadivel, M., Nandakumar, T., Lahiri, B.B., and Philip, J., 2024, Aqueous black seed (*Nigella sativa* L.) extract-mediated corrosion inhibition in mild steel exposed to 3.5% NaCl: Effect of temperature, pH, time, and *in situ* analysis using atomic force microscopy, *Trans. Indian Inst. Met.*, 77 (11), 3385–3396.

[46] Song, Z., Liu, L., Guo, M.Z., Cai, H., Liu, Q., Donkor, S., and Zhao, H., 2024, Inhibition performance of extract reinforcement corrosion inhibitor from waste *Platanus acerifolia* leaves in simulated concrete pore solution, *Case Stud. Constr. Mater.*, 20, e02992.

[47] Al-Amiery, A., Wan Isahak, W.N.R., and Al-Azzawi, W.K., 2024, Sustainable corrosion Inhibitors: A key step towards environmentally responsible corrosion control, *Ain Shams Eng. J.*, 15 (5), 102672.